Article

Cell Reports

RIP2 Gates TRAF6 Interaction with Death Receptor p75^{NTR} to Regulate Cerebellar Granule Neuron Survival

Graphical Abstract

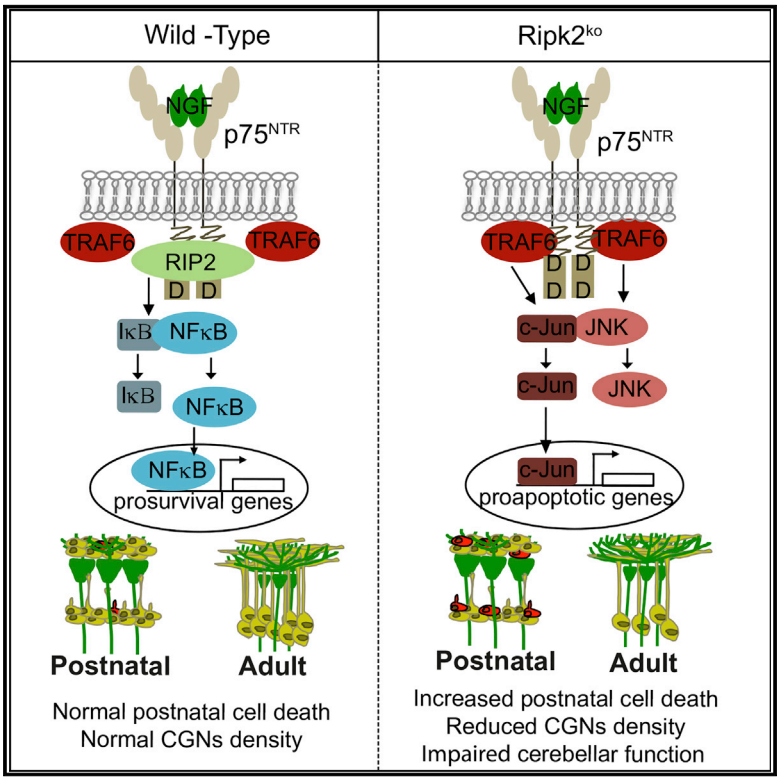

Highlights

- Deletion of RIP2 increased cerebellar granule neuron (CGN) apoptosis through p75^{NTR}
- RIP2 mutant mice show reduced CGN density and impaired cerebellar-dependent behavior
- RIP2 competes with TRAF6 for binding to p75^{NTR} intracellular domain
- RIP2 mutant CGNs have more TRAF6 associated with p75^{NTR} and increased JNK activity

Authors

Lilian Kisiswa, Diana Fernández-Suárez, Maria Christina Sergaki, Carlos F. Ibáñez

Correspondence

carlos.ibanez@ki.se

In Brief

Kisiswa et al. report that RIP2 gates the signaling output of p75^{NTR} by competing with TRAF6 for binding to the receptor death domain, increasing the survival of CGN in developing cerebellum. These results reveal a mechanism controlling CGN number and highlight how competitive interactions govern the logic of death receptor function.

Kisiswa et al., 2018, Cell Reports *24*, 1013–1024
July 24, 2018
https://doi.org/10.1016/j.celrep.2018.06.098

CellPress

Cell Reports
Article

RIP2 Gates TRAF6 Interaction with Death Receptor p75^{NTR} to Regulate Cerebellar Granule Neuron Survival

Lilian Kisiswa,[1] Diana Fernández-Suárez,[1] Maria Christina Sergaki,[1,4] and Carlos F. Ibáñez[1,2,3,5,*]
[1]Department of Cell and Molecular Biology, Karolinska Institute, Stockholm 17177, Sweden
[2]Department of Physiology, National University of Singapore, Singapore 117597, Singapore
[3]Life Sciences Institute, National University of Singapore, Singapore 117456, Singapore
[4]Present address: IMP Research Institute of Molecular Pathology, Vienna, Austria
[5]Lead Contact
*Correspondence: carlos.ibanez@ki.se
https://doi.org/10.1016/j.celrep.2018.06.098

SUMMARY

Cerebellar granule neurons (CGNs) undergo programmed cell death during the first postnatal week of mouse development, coincident with sustained expression of the death receptor p75^{NTR}. Although ablation of p75^{NTR} does not affect CGN cell death, deletion of the downstream effector RIP2 significantly increases CGN apoptosis, resulting in reduced adult CGN number and impaired behaviors associated with cerebellar function. Remarkably, CGN death is restored to basal levels when p75^{NTR} is deleted in RIP2-deficient mice. We find that RIP2 gates the signaling output of p75^{NTR} by competing with TRAF6 for binding to the receptor intracellular domain. In CGNs lacking RIP2, more TRAF6 is associated with p75^{NTR}, leading to increased JNK-dependent apoptosis. In agreement with this, pharmacological inhibition or genetic ablation of TRAF6 restores cell death levels in CGNs lacking RIP2. These results reveal an unexpected mechanism controlling CGN number and highlight how competitive interactions govern the logic of death receptor function.

INTRODUCTION

Death receptors are characterized by the presence of a globular 6-helix bundle domain in their intracellular region known as the "death domain" (Ferrao and Wu, 2012; Park et al., 2007). Prototypical death receptors include the tumor necrosis factor receptor 1 (TNFR1), the Fas receptor (CD95), and the p75 neurotrophin receptor (p75^{NTR}) (also known as nerve growth factor receptor [NGFR], TNFRSF16, and CD271). Lacking enzymatic activity, death receptors form complexes with intracellular effectors and signal by binding or releasing different components. Death receptor signaling can involve multiple pathways, sometimes with opposing functions. For example, TNFR1 and p75^{NTR} can induce apoptosis through a pathway that requires JNK (c-Jun N-terminal kinase) activity (Friedman, 2000; Wicovsky et al., 2007; Yoon et al., 1998) or promote survival via the transcription factor NF-κB (nuclear factor kappa-B) (Carter et al., 1996; Khursigara et al., 2001; McCarthy et al., 1998; Vicario et al., 2015). Although the signaling cascades leading to these effects have been characterized in some detail, the underlying logic that determines which pathway becomes predominant, and under which circumstances, remains unclear. Death domains are relatively small protein domains (typically less than 10 kDa), although many of their intracellular interactors are often much larger (60 kDa or more), so it is likely that many of these interactions are mutually exclusive.

p75^{NTR} is highly expressed in the developing nervous system and upon injury or neurodegeneration in the adult, where it functions as a receptor for members of the neurotrophin family, such as nerve growth factor (NGF) (Dechant and Barde, 2002; Roux and Barker, 2002). The receptor is present at the neuronal plasma membrane as a dimer stabilized by both covalent and non-covalent interactions (Vilar et al., 2009). The p75^{NTR} death domain forms low-affinity homodimers (Lin et al., 2015) that dissociate upon NGF binding (Vilar et al., 2009) to allow the recruitment of intracellular effectors, such as RIP2 (receptor interacting protein 2), a member of the RIP kinase family. RIP2 is a necessary component linking p75^{NTR} to the NF-κB pathway (Khursigara et al., 2001), an activity that has been associated to cell survival in some cell types, such as Schwann cells (Khursigara et al., 2001) and cerebellar granule neurons (CGNs) (Vicario et al., 2015). Another major intracellular effector of p75^{NTR}, TRAF6 (TNFR-associated factor 6), binds to juxtamembrane sequences outside the death domain (Khursigara et al., 1999). TRAF6 has primarily been implicated in the ability of p75^{NTR} to induce cell death in a JNK-dependent manner (Geetha et al., 2005; Yeiser et al., 2004). It is not understood how these two signaling pathways are organized on the p75^{NTR} molecule or whether they interact, something that ought to be critical, given that they mediate opposed functional outcomes.

The mechanisms that determine the final number of neurons in the mature CNS are incompletely understood. Programmed cell death is a crucial event required for the elimination of excess neurons and the formation of proper connections. It is a tightly regulated process, involving several families of extracellular factors, including the neurotrophins and their receptors. However, although the neurotrophic theory has provided a powerful

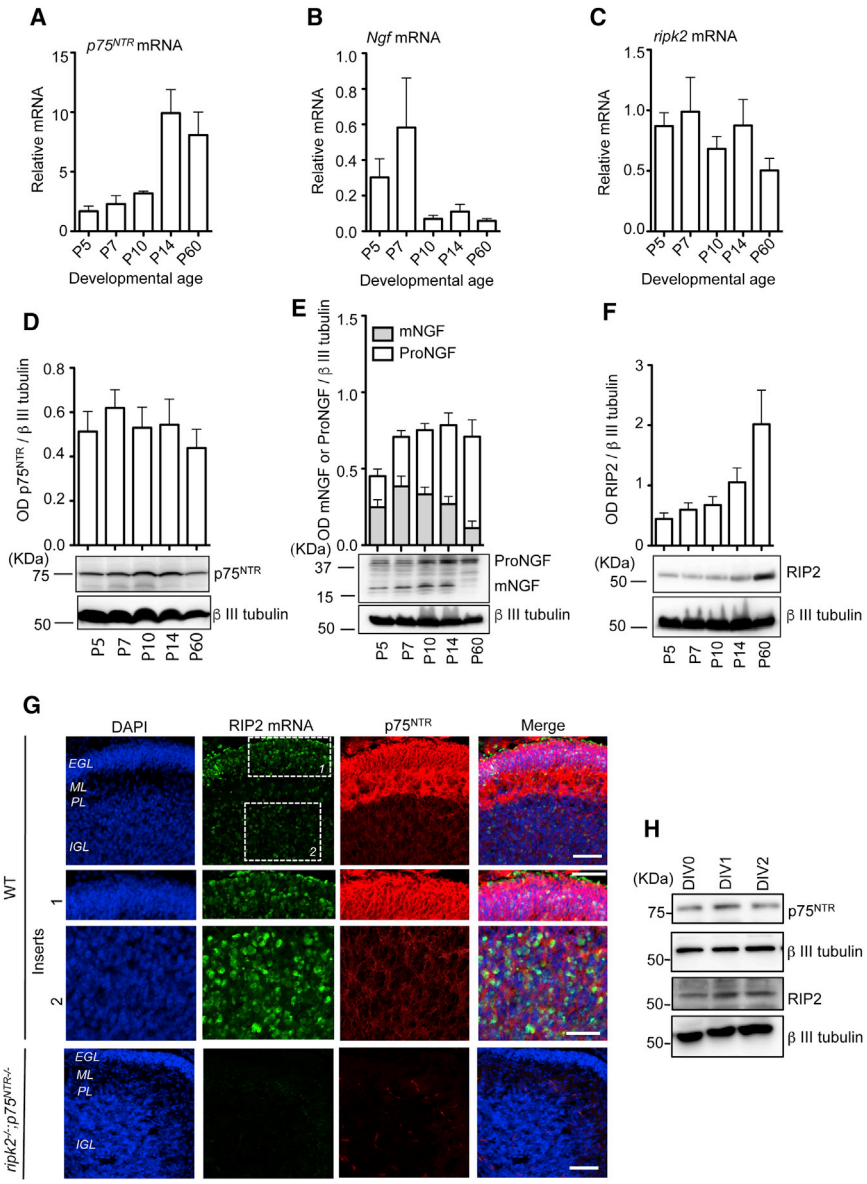

Figure 1. Expression of p75^{NTR}, NGF, and RIP2 during Postnatal Cerebellar Development

(A–C) *p75^{NTR}* mRNA (A), *Ngf* mRNA (B), and *ripk2* mRNA (C) quantification relative to 18S RNA levels in cerebellum at the indicated postnatal (P) ages (mean ± SEM of data from 5 cerebella at each age).

(D–F) Representative immunoblots and quantification of p75^{NTR} (D) mature (mNGF), proNGF (E), and RIP2 (F) protein in total cerebellar protein extracts at the indicated ages (mean ± SEM densitometry from six experiments; representative blots are shown).

(G) Micrographs of representative P7 cerebellum sections labeled with RIP2 antisense *in situ* hybridization probe, anti-p75^{NTR} antibody, and counterstained with DAPI. The scale bars represent 50 μm.

(H) Immunoblots showing the expression of p75^{NTR} and RIP2 in CGNs cultured for the indicated days *in vitro* (DIV).

framework to explain programmed cell death in the peripheral nervous system, it has been far less applicable in the brain. CGNs comprise over half of all the neurons in the mammalian brain. They are thought to encode ongoing sensorimotor as well as cognitive information to allow associative learning at their postsynaptic targets, the Purkinje neurons (Becker and Person, 2017). In the mouse cerebellum, CGNs undergo programmed cell death during the first postnatal week (Wood et al., 1993), but it is unclear how this process is regulated.

In this study, we have examined the cerebella of mice lacking RIP2 and found increased CGN apoptosis that was mediated by the p75^{NTR} death receptor. Mechanistically, this resulted from increased association of TRAF6 with p75^{NTR}, leading to enhanced JNK activity in CGNs lacking RIP2. These findings reveal an unexpected hierarchical relationship between the RIP2 and TRAF6 pathways in the control of CGN survival through the p75^{NTR} death receptor.

RESULTS

Expression of p75^{NTR}, NGF, and RIP2 during Postnatal Cerebellar Development

Expression of the mRNAs encoding p75^{NTR}, NGF, and RIP2 during cerebellar postnatal development (from postnatal day 5 [P5] to P60) was analyzed by qPCR. All three transcripts were detected in mouse cerebellum, although they showed different dynamic patterns of expression. p75^{NTR} mRNA levels were sustained during the first two postnatal weeks but increased thereafter (Figure 1A). On the other hand, NGF mRNA was highest in the first postnatal week and normalized at lower levels after the second week (Figure 1B). RIP2 mRNA expression remained fairly constant during the interval examined (Figure 1C). Protein levels, examined by quantitative immunoblotting, showed a few differences compared to the corresponding mRNA patterns. p75^{NTR} expression was constant and sustained through the ages examined (Figure 1D). The levels of mature NGF declined after the second postnatal week (Figure 1E). At the same time, the levels of proNGF, the uncleaved NGF precursor protein (Lee et al., 2001), markedly increased during the second week and remained high thereafter (Figure 1E). Interestingly, RIP2 protein levels were seen to increase steadily during this period, with maximal levels in young adult mice (Figure 1F). Using combined *in situ* hybridization (for RIP2 mRNA) and immunohistochemistry (for p75^{NTR}) in sections of P7 cerebella, we detected colocalization of the two molecules

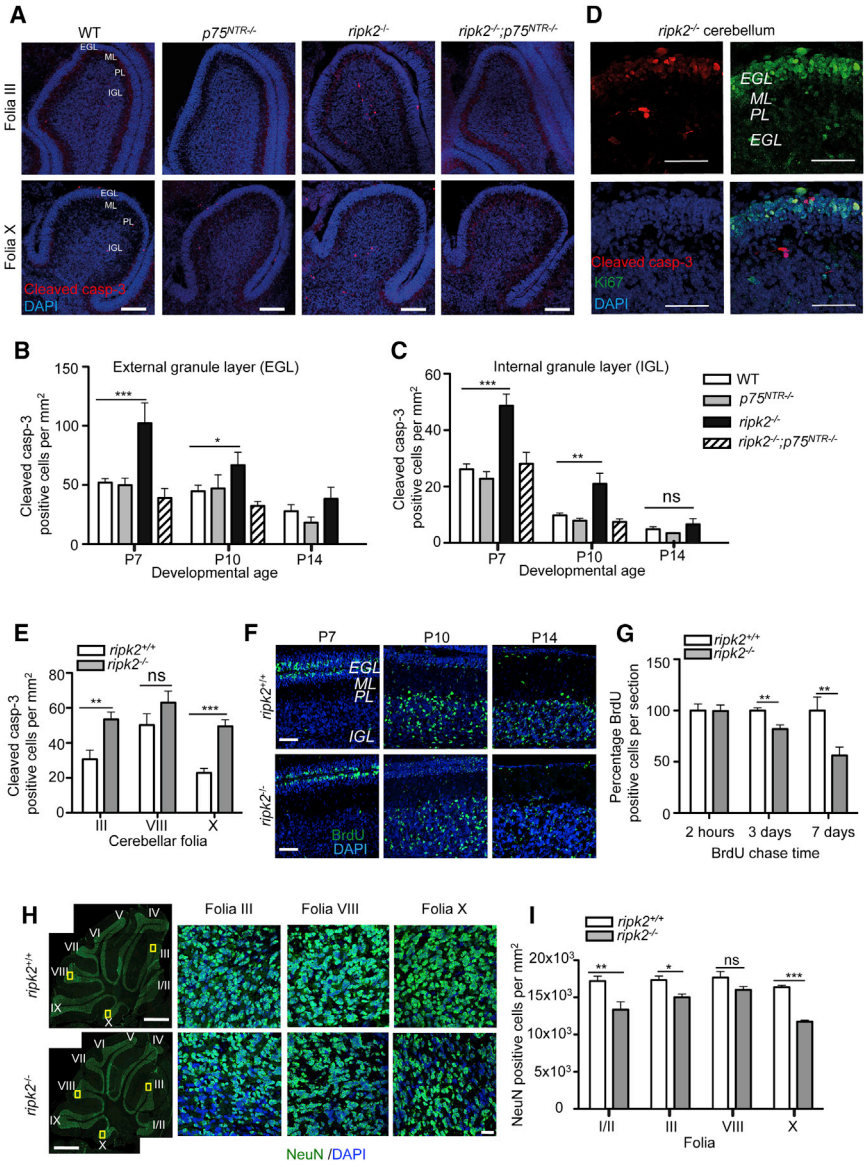

Figure 2. Increased Cell Death in CGNs of Mice Lacking RIP2 Is Mediated by p75^{NTR}

(A) Representative micrographs of sections of cerebellar folia III and X from P7 wild-type (WT), p75$^{NTR-/-}$, ripk2$^{-/-}$, and ripk2$^{-/-}$; p75$^{NTR-/-}$ mice labeled with antibodies to cleaved caspase 3 and counterstained with DAPI (images were selected from 270 WT, 70 p75$^{NTR-/-}$, 90 ripk2$^{-/-}$ and 60 ripk2$^{-/-}$; p75$^{NTR-/-}$ cerebella). The scale bars represent 100 μm.

(B and C) Quantification of cleaved-caspase-3-positive cells in external granule layer (B) and internal granule layer (C) of cerebella from P7, P10, and P14 WT, p75$^{NTR-/-}$, ripk2$^{-/-}$, and ripk2$^{-/-}$; p75$^{NTR-/-}$ mice. The results are presented as mean ± SEM from 24 WT, 7 p75$^{NTR-/-}$, 8 ripk2$^{-/-}$, and 6 ripk2$^{-/-}$; p75$^{NTR-/-}$ P7 mice; 18 WT, 6 p75$^{NTR-/-}$, 8 ripk2$^{-/-}$, and 6 ripk2$^{-/-}$; p75$^{NTR-/-}$ P10 mice; and 10 WT, 6 p75$^{NTR-/-}$, and 6 ripk2$^{-/-}$ P14 mice (*$p < 0.05$ and ***$p < 0.001$ compared to control; **$p < 0.01$; two-way ANOVA followed by Bonferroni multiple comparisons test).

(D) Representative micrographs of sections through cerebellar folium III labeled with antibodies to cleaved caspase 3, Ki67, and counterstained with DAPI. The scale bars represent 50 μm.

(E) Quantification of cells positive for cleaved caspase 3 in IGL of folia III, VIII, and X of P7 wild-type (ripk2$^{+/+}$) and ripk2$^{-/-}$ mutant mice. Mean ± SEM of data from 7 ripk2$^{+/+}$ mice and 7 ripk2$^{-/-}$ (**$p < 0.01$ and ***$p < 0.001$ compared to control; unpaired Student's t test) is shown.

(F) Representative micrographs of cerebellar sections from P7, P10, and P14 ripk2$^{+/+}$ and ripk2$^{-/-}$ mice injected with BrdU at P7. Images were selected from 200 images per genotype and age. Sections were probed for BrdU with antibodies and counterstained with DAPI. The scale bars represent 50 μm.

(G) Percentage total BrdU-positive cells per section after 2 hr, 3 days, and 7 days of a BrdU pulse in ripk2$^{+/+}$ and ripk2$^{-/-}$ mice. Mean ± SEM of data from 5 ripk2$^{+/+}$ and 5 ripk2$^{-/-}$ mice per age (**$p < 0.01$ compared to control, unpaired Student's t test) is shown.

(H) Representative micrographs of adult cerebella demo ripk2$^{+/+}$ and ripk2$^{-/-}$ mice showing the different folia and the areas used for quantification (boxed, left panel) and 63× magnification images from folia III, VIII, and X (right panels) labeled with antibodies against NeuN and counterstained with DAPI. The scale bars represent 500 μm for images in the first panel and 20 μm for the high-magnification images. Images shown were selected from 50 images per genotype and selected folia. The image in the first panel was created as a montage of several images using the ImageMontage plugin in NIH ImageJ software.

(I) Quantification of NeuN-positive cells per mm^2 in ripk2$^{+/+}$ and ripk2$^{-/-}$ mice. Mean ± SEM of data from 3 ripk2$^{+/+}$ and 3 ripk2$^{-/-}$ mice for folia I/II; 7 ripk2$^{+/+}$ and 7 ripk2$^{-/-}$ mice for folia III; 8 ripk2$^{+/+}$ and 7 ripk2$^{-/-}$ mice for folia VIII; and 8 ripk2$^{+/+}$ and 8 ripk2$^{-/-}$ mice for folia X (*$p < 0.05$; **$p < 0.01$; and ***$p < 0.001$ compared to control; unpaired Student's t test) is shown.

in the external and internal granule layers (EGL and IGL, respectively; Figure 1G). As previously described (Friedman et al., 1991), p75^{NTR} was abundantly expressed by Purkinje cells. However, no RIP2 mRNA expression could be detected in those cells (Figure 1G). Importantly, no signal could be detected for either marker in double mutant mice lacking RIP2 and p75^{NTR} (Figure 1G). As the EGL is known to exclusively generate CGNs (Carletti and Rossi, 2008), these data indicate that these neurons co-express p75^{NTR} and RIP2. This was confirmed by immunoblotting in cell lysates of pure cultures of P5 CGNs (Figure 1H).

Increased Cell Death in CGNs of Mice Lacking RIP2 Is Mediated by p75^{NTR}

We investigated cell death in cerebella of mutant mice lacking RIP2 (ripk2$^{-/-}$) by immunohistochemistry for cleaved caspase 3 at P7, P10, and P14. ripk2$^{-/-}$ mutant mice showed increased cleaved caspase 3 immunoreactivity in both the EGL, which harbors proliferating CGNs, and IGL, containing mature CGNs (Figures 2A–2C). This was most prominent at P7, the height of CGNs programmed cell death. We assessed whether CGNs marked by cleaved caspase 3 included mitotic cells by immunostaining

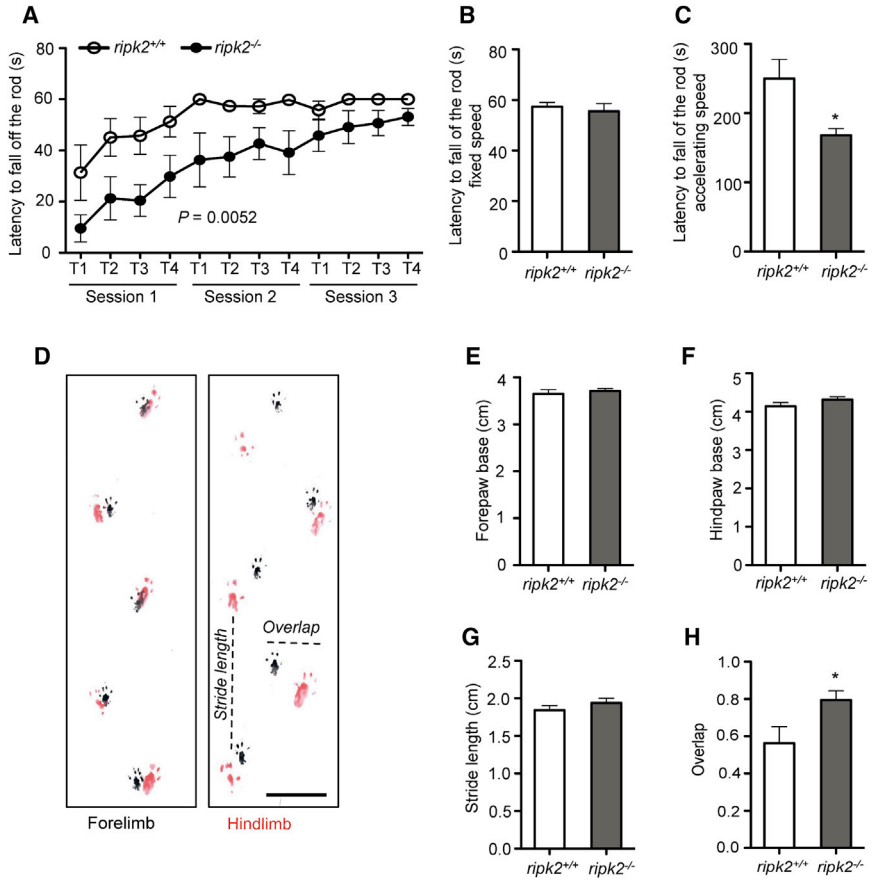

Figure 3. Impaired Motor Behaviors Associated with Cerebellar Function in Mice Lacking RIP2

(A) Motor learning curve of RIP2 mutants and their controls subjected to 4 trials per session on rotarod (20 rpm fix speed; max 60 s; inter-trial time 30 min). Mean ± SEM of data from 8 ripk2$^{+/+}$ and 8 ripk2$^{-/-}$ mice is shown. p = 0.0052; two-way ANOVA.

(B and C) Rotarod performance at fixed speed (20 rpm; B) and at accelerating speed (from 4 to 40 rpm; C). Mean ± SEM of data from 8 ripk2$^{+/+}$ and 8 ripk2$^{-/-}$ 6-month-old mice is shown. *p < 0.05 compared to control; unpaired Student's t test.

(D) Paw prints of the fore and the hind paws for representative runs by male ripk2$^{+/+}$ and ripk2$^{-/-}$ mice and example of parameters measured in footprint analysis. Scale bar, 1 cm.

(E–H) Bar graphs showing forepaw base (E), hind paw base (F), stride length (G), and overlap (H) parameters in ripk2$^{+/+}$ and ripk2$^{-/-}$ mice. Mean ± SEM of data from 8 ripk2$^{+/+}$ and 8 ripk2$^{-/-}$ mice. *p < 0.05 compared to control; unpaired Student's t test.

sections of P7 cerebella with the proliferation marker Ki67. Both Ki67-positive and negative CGNs were marked by cleaved caspase 3 (Figure 2D), indicating that RIP2 deficiency affected the survival of both mitotic and postmitotic CGNs. Intriguingly, we found that the augmented cell death observed in CGNs of mice lacking RIP2 was restored to wild-type levels in double mutants lacking both RIP2 and p75^{NTR} (ripk2$^{-/-}$;p75$^{NTR-/-}$; Figures 2A–2C). Deletion of p75^{NTR} alone did not have an effect on CGN cell death (Figures 2A–2C). Together, these data suggested that the increased cell death observed in cerebella of mice lacking RIP2 was mediated by p75^{NTR}.

In order to further characterize CGN death in ripk2$^{-/-}$ mutant mice, we examined cleaved caspase 3 in cerebellar regions known to receive different afferent innervation. A significant increase in cells immunoreactive for cleaved caspase 3 was found in folia I/II (spino-cerebellum) and X (vestibular-cerebellum; Figure 2E). Cell death was less pronounced in folia VIII (ponto-cerebellum) of ripk2$^{-/-}$ mutant mice. As it has been reported that p75^{NTR} can regulate CGN proliferation (Zanin et al., 2016), we performed bromodeoxyuridine (BrdU) pulse-chase experiments to assess whether RIP2 deletion had any impact on proliferation or migration of CGNs. BrdU was injected subcutaneously in ripk2$^{+/+}$ and ripk2$^{-/-}$ pups at P7, a time of high CGN proliferation in the EGL (Carletti and Rossi, 2008), and BrdU-positive cells were quantified 2 hr, 3 days, and 7 days later. No difference between genotypes was observed 2 hr post-injection (EGL; Figures 2F and 2G), indicating that there were no changes in cell proliferation in CGNs of the mutant cerebellum. This was confirmed by assessing the ratio of phospho-histone H3 to Ki67 staining in sections of P7 in ripk2$^{+/+}$ and ripk2$^{-/-}$ cerebella (Figures S1A and S1B). The number of BrdU-labeled cells 3 days post-injection (some in EGL, most in IGL) was reduced in the mutants, and this reduction was even more pronounced 7 days after BrdU injection (almost all in IGL; Figure 2G). Although reduced in number, the relative distribution of BrdU-labeled cells among different cerebellar layers was not different between wild-type and mutant at any time point (Figures S1C–S1F), confirming that the deficits observed in ripk2$^{-/-}$ mice are in CGN survival and not migration. These deficits were maintained in the cerebellum of adult (P60) ripk2$^{-/-}$ mice, as indicated by a decrease of the overall number of NeuN-positive neurons in different cerebellar folia (Figures 2H and 2I).

Impaired Motor Behaviors Associated with Cerebellar Function in Mice Lacking RIP2

Adult (6-month-old) ripk2$^{+/+}$ and ripk2$^{-/-}$ mice were subjected to a battery of behavioral tests to measure exploratory activity (Foti et al., 2010), anxiety (Apps and Strata, 2015), gait (Vinueza Veloz et al., 2015), and motor learning and function (De Zeeuw and Ten Brinke, 2015; Sergaki et al., 2017). We did not detect significant differences between genotypes in the open-field test (Figures S2A–S2C), light-dark box test (Figures S2D–S2F), or elevated plus maze (Figures S2G–S2I), indicating normal locomotor activity and exploratory and anxiety behaviors in ripk2$^{-/-}$ mutant mice. However, there were significant differences in the learning curves of rotarod training sessions between the two genotypes (Figure 3A). After the training, although ripk2$^{-/-}$ mutants were

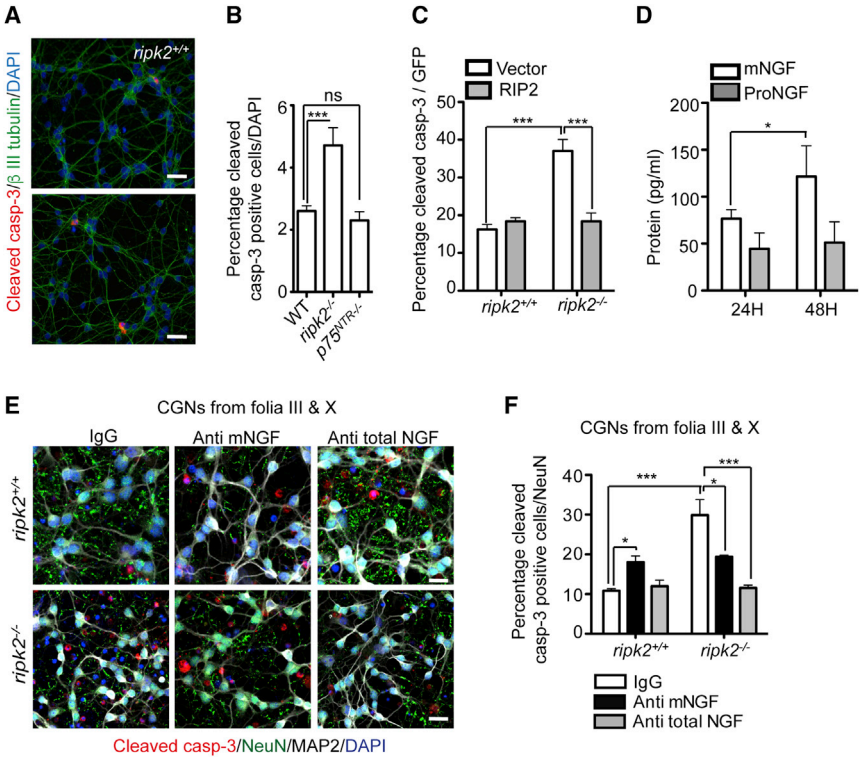

Figure 4. RIP2 Regulates CGN Survival Cell Autonomously by Gating p75^{NTR} Responsiveness to Endogenous NGF

(A) Image of representative cultures of P7 CGNs from ripk2$^{+/+}$ and ripk2$^{-/-}$ mice after 2 DIV stained as indicated. The scale bars represent 20 μm. Images were selected from 60 images per genotype.

(B) Percentage of cells positive for cleaved caspase 3 in cultured wild-type, ripk2$^{-/-}$, and p75$^{NTR-/-}$ CGNs. Mean ± SEM of data from 5 separate cultures is shown (***p < 0.001 compared to control; unpaired Student's t test).

(C) Quantification of cells positive for cleaved caspase 3 in ripk2$^{+/+}$ and ripk2$^{-/-}$ CGNs transfected with either empty vector or RIP2 plasmid. Mean ± SEM of data from 4 separate cultures is shown (***p < 0.001 two-way ANOVA followed by Bonferroni test).

(D) Concentration of secreted mature NGF (mNGF) and proNGF by cultured wild-type CGNs at a density of 1,000,000 neurons per well in a 48-well plate. Mean ± SEM of data from 5 separate cultures is shown (*p < 0.05 compared to control; unpaired Student's t test).

(E) Representative images of P7 ripk2$^{+/+}$ and ripk2$^{-/-}$ CGNs dissected from folia III and X cultured for 2 DIV and treated with IgG, anti mNGF, or anti-total NGF. Images were selected from 30 images per genotype. The scale bars represent 50 μm.

(F) Percentage cells positive for cleaved caspase 3 in cultured CGNs from ripk2$^{+/+}$ and ripk2$^{-/-}$ mice treated with IgG control (1 μg/mL), anti mNGF (1 μg/mL), or anti total NGF (1 μg/mL) antibodies for 24 hr. Mean ± SEM of data from five separate cultures per genotype and condition is shown (*p < 0.05; ***p < 0.001; two-way ANOVA followed by Bonferroni test).

able to stay on the rod at the fix speed of 20 rpm (Figure 3B), they fell more readily than wild-type littermates on a rod accelerating from 4 to 40 rpm (Figure 3C). In the gait test, forepaw and hind paw base as well as stride length were similar in mutant and control mice (Figures 3D–3G), but the overlap between the forepaw and hind paw was increased in ripk2$^{-/-}$ mutant mice compared to wild-type littermates (Figure 3H), indicating gait defects. Mutant mice did not show tremors or signs of ataxia. Together, these findings indicate impairment in several motor behaviors associated with cerebellar function in mice lacking RIP2.

RIP2 Regulates CGN Survival Cell Autonomously by Gating p75^{NTR} Responsiveness to Endogenous NGF

After 3 days *in vitro* (3 DIV), CGNs isolated from P7 ripk2$^{-/-}$ mutant mice showed a significant increase in cleaved caspase 3 immunoreactivity compared to those derived from wild-type controls or p75$^{NTR-/-}$ mutant mice (Figures 4A and 4B), in agreement with our findings *in vivo*. Re-expression of RIP2 in ripk2$^{-/-}$ mutant neurons by transfection restored cleaved caspase 3 immunoreactivity to wild-type levels (Figure 4C), suggesting that RIP2 can regulate CGN survival cell autonomously. We found that both mature NGF (mNGF) and proNGF were endogenously produced in our CGN cultures and could be detected in CGN supernatants after 1 and 2 DIV (Figure 4D). There were no differences between the levels of mNGF produced in wild-type and ripk2$^{-/-}$ mutant CGN cultures (Figure S3A). We then tested the functional relevance of the endogenously produced NGF for CGNs survival using function-blocking antibodies (Figures 4E and 4F). Because untransfected CGNs extracted from the whole cerebellum had shown low levels of cell death in culture (Figure 4B), we prepared CGNs from cerebellar folia III and X, as these were the most sensitive to *ripk2* deletion (Figure 2E). This significantly increased the dynamic range of the assay (Figure 4F), allowing us to more accurately assess the effects of the different blocking antibodies. Antibody MAB256 has been shown to preferentially bind to mNGF (Malerba et al., 2015) and to block its function (Dollé et al., 2003), and antibody ALM006 can block the activities of both NGF isoforms (Ding et al., 2015; Pundavela et al., 2015). Blocking mNGF with MAB256 induced cleaved caspase 3 immunoreactivity in wild-type CGNs maintained for 24 hr with the antibody (solid bars in Figure 4F), suggesting that endogenous mNGF has a pro-survival function in these cultures. As before, CGNs derived from ripk2$^{-/-}$ mutant mice showed increased cell death under control conditions (open bars in Figure 4F), but in this case, addition of the anti-mNGF blocking antibody reduced the levels of cleaved caspase 3 (solid bars in Figure 4F). On the other hand, blocking the function of both mNGF and proNGF with ALM006 had no effect on wild-type neurons but completely counteracted the effect of the RIP2 mutation on CGN death, restoring it to wild-type levels (gray bars in Figure 4F). Thus, in the presence of RIP2 (i.e., wild-type CGNs), mNGF has pro-survival and proNGF pro-death activity, but both isoforms can induce apoptosis if RIP2 is missing (i.e., ripk2$^{-/-}$ mutant CGNs). This suggested

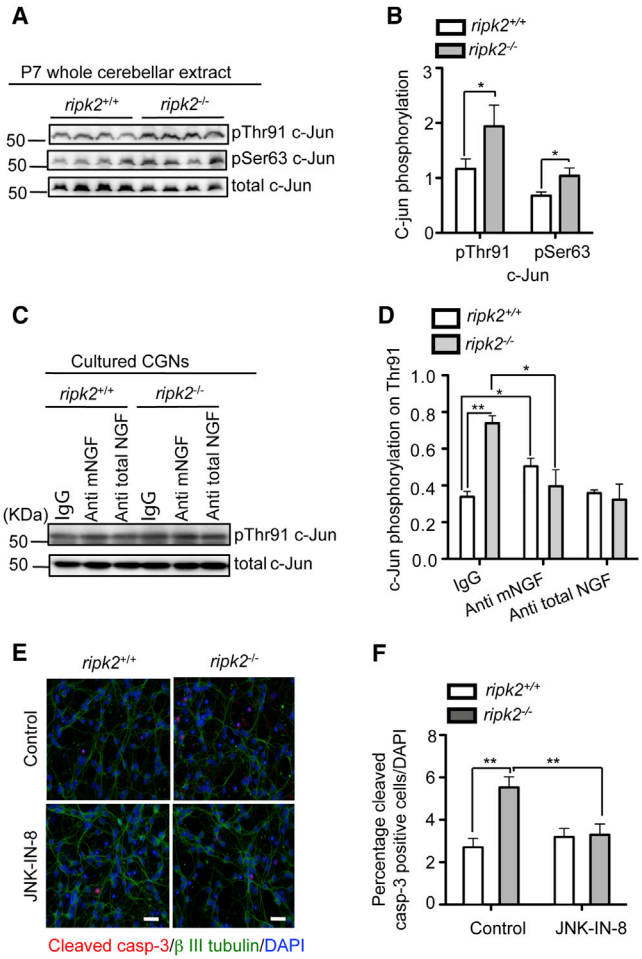

Figure 5. CGN Cell Death Induced by Lack of RIP2 Is Dependent on JNK Activity

(A) Representative immunoblots probed with antibodies to phospho-cJun (Thr91), phospho-cJun (Ser63), total cJun, and β III tubulin. Each lane corresponds to cerebellar extracts from different animals. MW marker indicated in kDa.

(B) Quantification of cJun phosphorylation in whole cerebellar extracts from P7 ripk2$^{+/+}$ and ripk2$^{-/-}$ mice. Mean ± SEM of densitometry scans derived from samples of 6 ripk2$^{+/+}$ and ripk2$^{-/-}$ mice is shown (*p < 0.001; one-way ANOVA followed by Bonferroni test).

(C and D) Immunoblots probed with phospho-cJun (Thr91) and total cJun (C) and quantification of c-Jun phosphorylation (D) in cultured P7 CGNs from ripk2$^{+/+}$ and ripk2$^{-/-}$ mice treated with IgG control (1 μg/mL), anti-mNGF (1 μg/mL), or anti total NGF (1 μg/mL) antibodies for 30 min. Mean ± SEM of densitometry from 3 experiments is shown (*p < 0.05; **p < 0.01; two-way ANOVA followed by Bonferroni test).

(E) Representative micrographs of cultured CGNs from ripk2$^{+/+}$ and ripk2$^{-/-}$ mice after 2 DIV followed by treatment with vehicle (control) or JNK-8 inhibitor (JNK-IN-8 at 3 μM) labeled with antibodies to cleaved caspase 3 and β III tubulin and counterstained with DAPI. Images were selected from 83 images per genotype and condition. The scale bars represent 20 μm.

(F) Percentage of cells positive for cleaved caspase 3 in cultured CGNs from ripk2$^{+/+}$ and ripk2$^{-/-}$ mice treated with vehicle (control) or JNK-IN-8 for 24 hr. Mean ± SEM of data from four separate cultures is shown (**p < 0.01 compared to control; unpaired Student's t test).

that the pro-survival effects of mNGF are RIP2 dependent, and the increased cell death observed after blocking mNGF is mediated by proNGF. The anti-mNGF antibody did not increase caspase 3 activity in p75$^{NTR-/-}$ mutant neurons like it did in wild-type cells (Figure S3B). This is in agreement with the idea that the increased apoptosis induced by anti-mNGF in wild-type CGNs is mediated by interaction of endogenous proNGF with p75^{NTR}.

CGN Cell Death Induced by Lack of RIP2 Is Dependent on JNK Activity

Because of its prominent role in death receptor signaling (Friedman, 2000; Wicovsky et al., 2007; Yoon et al., 1998), we investigated the involvement on the JNK pathway in CGN cell death induced by absence of RIP2. Phosphorylation of c-Jun, a major JNK target, on Thr^{91} and Ser^{63} was increased in whole tissue extracts of P7 cerebellum from ripk2$^{-/-}$ mutant mice compared to ripk2$^{+/+}$ littermate controls (Figures 5A and 5B). Increased c-Jun phosphorylation on Thr^{91}, a modification that has been specifically linked to JNK-mediated apoptosis in CGNs (Reddy et al., 2013), was also observed in cultured CGNs lacking RIP2 (Figures 5C and 5D). This was reduced upon treatment with function-blocking antibodies against mNGF or total NGF (Figure 5D). Moreover, wild-type ripk2$^{+/+}$ neurons treated with anti-mNGF, but not with anti-total NGF, blocking antibody also showed elevated c-Jun phosphorylation in Thr^{91} (Figure 5D), in agreement with the results of caspase 3 activation. Immunoreactivity for activated caspase 3 in cultures of ripk2$^{-/-}$ mutant CGNs was restored to basal levels upon treatment with the specific JNK inhibitor JNK-IN-8 (Zhang et al., 2012; Figures 5E and 5F). Together, these results support the involvement of the JNK pathway in CGN cell death induced by lack of RIP2.

RIP2 Gates the Interaction of TRAF6 with p75^{NTR} to Regulate CGN Survival

Given the involvement of TRAF6 in the regulation of JNK activity downstream of death receptors, we investigated the expression of TRAF6 during cerebellum development and its interaction with p75^{NTR} in wild-type CGNs and CGNs lacking RIP2. TRAF6 was most highly expressed during the first week of postnatal cerebellar development (Figure 6A), coincident with the peak of CGN cell death. In cultures of wild-type CGNs, treatment with mNGF induced association of RIP2 with p75^{NTR} (Figures 6B and 6C) but did not significantly affect the interaction of TRAF6 with the receptor (Figures 6B and 6D). mNGF increased the nuclear translocation of the p65^{NF-kB} subunit in wild-type, but not ripk2$^{-/-}$ mutant, CGNs (Figures S4A and S4B), in agreement with the role of RIP2 in this pathway. In contrast to mNGF, proNGF increased binding of TRAF6 to p75^{NTR} (Figures 6B and 6D) but had no effect on RIP2 (Figures 6B and 6C). Immunoprecipitation of p75^{NTR} from P7 cerebellar extracts consistently recovered higher levels of TRAF6 in ripk2$^{-/-}$ mutant mice compared to wild-type controls (Figures 6E and 6F). These results were confirmed using the proximity ligation assay (PLA) in cultured CGNs from wild-type and ripk2$^{-/-}$ mice (Figure 6G and open bars in Figure 6H). In line with these results, reintroduction of RIP2 by transfection in ripk2$^{-/-}$ CGNs restored the interaction of TRAF6 with p75^{NTR} to wild-type levels (gray bars in

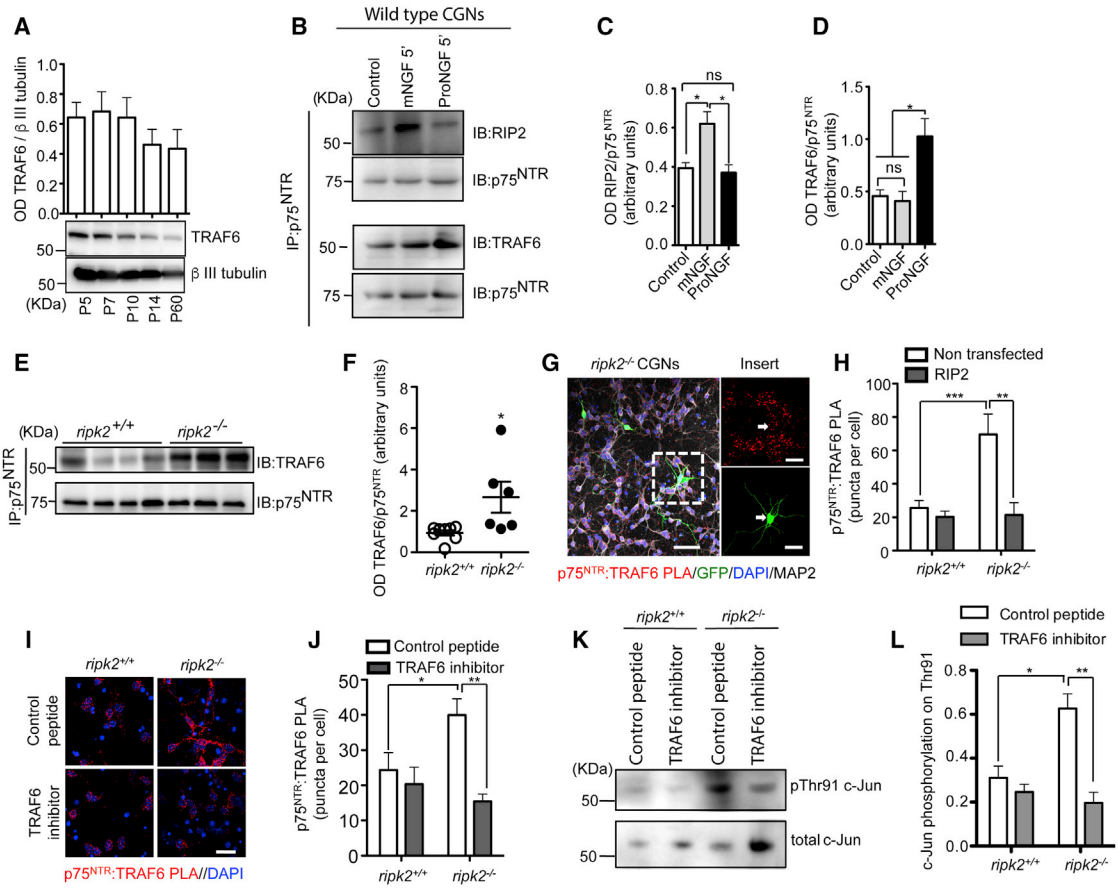

Figure 6. RIP2 Gates the Interaction of TRAF6 with p75^{NTR}

(A) Representative western blots and quantification of TRAF6 protein in total cerebellar extracts at the indicated developmental ages (mean ± SEM of densitometry from 3 experiments; representative blots were selected from these 3 experiments).

(B) Representative immunoblots of p75^{NTR} immunoprecipitation of protein from cultured P7 wild-type CGNs stimulated with either mNGF or ProNGF for 5 min and then probed with antibodies to RIP2, TRAF6, or p75^{NTR}. IB, immunoblotting; IP, immunoprecipitation.

(C and D) Quantification of RIP2 (C) and TRAF6 (D) in p75^{NTR} immunoprecipitates from P7 wild-type CNGs after treatment with mNGF or ProNGF. Mean ± SEM of densitometry from 4 separate cultures is shown (*p < 0.05 one-way ANOVA followed by Bonferroni test; ns, not significantly different).

(E) Representative immunoblots of p75^{NTR} immunoprecipitates from cerebellar lysates of P7 ripk2$^{+/+}$ and ripk2$^{-/-}$ mice probed with antibodies to TRAF6 and re-probed for p75^{NTR}.

(F) Quantification of TRAF6 in p75^{NTR} immunoprecipitates from cerebellar lysates of P7 ripk2$^{+/+}$ and ripk2$^{-/-}$ mice. Mean ± SEM of densitometry from 6 ripk2$^{+/+}$ and 6 ripk2$^{-/-}$ mice (*p < 0.05 compared to control; unpaired Student's t test).

(G) Micrographs of p75^{NTR}/TRAF6 PLA (red) in transfected (GFP, green) ripk2$^{-/-}$ CGNs counterstained with antibodies to MAP2 and with DAPI. Images were selected from 40 images per genotype and condition from 5 separate experiments. Arrow shows ripk2$^{-/-}$ CGN transfected with RIP2 plasmid. The scale bars represent 20 μm.

(H) Quantification of p75:TRAF6 PLA puncta in control or RIP2-transfected ripk2$^{+/+}$ and ripk2$^{-/-}$ CGNs. Mean ± SEM of data from 4 separate cultures is shown (**p < 0.01 two-way ANOVA followed by Bonferroni test; ***p < 0.001).

(I) Micrographs of p75^{NTR}/TRAF6 PLA (red) in ripk2$^{+/+}$ and ripk2$^{-/-}$ CGNs cultured for 2 DIV and treated with control peptide (Ctr Pep; 30 μM) or TRAF6 decoy peptide (TRAF6in; 30 μM) counterstained with DAPI. Images were selected from 30 images per genotype and condition from 4 separate experiments. The scale bar represents 20 μm.

(J) Quantification of p75^{NTR}:TRAF6 PLA puncta in ripk2$^{+/+}$ and ripk2$^{-/-}$ CGNs treated with control peptide or TRAF6 inhibitor (decoy) peptide. Mean ± SEM of data from 3 separate cultures is shown (*p < 0.05; **p < 0.01 two-way ANOVA followed by Bonferroni test).

(K and L) Immunoblots probed with antibodies to phospho-cJun (Thr91) or total c-Jun (K) and quantification of c-Jun phosphorylation on Thr91 (L) in cultured P7 ripk2$^{+/+}$ and ripk2$^{-/-}$ CGNs treated with control peptide (control Pep; 30 μM) or TRAF6 decoy peptide (TRAF6 inhibitor; 30 μM) for 15 min. Mean ± SEM of densitometry from 3 experiments is shown (*p < 0.05; **p < 0.01; compared to control; two-way ANOVA followed by Bonferroni test).

Figure 6H), a condition that also restored normal levels of cell death in the mutant neurons, as shown earlier (Figure 4C). Interestingly, treatment with a cell-permeable TRAF6 decoy peptide that masks the TRAF6 binding site in death receptors (Ye et al., 2002) also reduced binding of TRAF6 to p75^{NTR} in ripk2$^{-/-}$ CGNs as assessed by PLA (Figures 6I and 6J). Under these conditions, the TRAF6 decoy peptide also reduced c-Jun phosphorylation on Thr91 in the mutant neurons (Figures 6K and 6L)

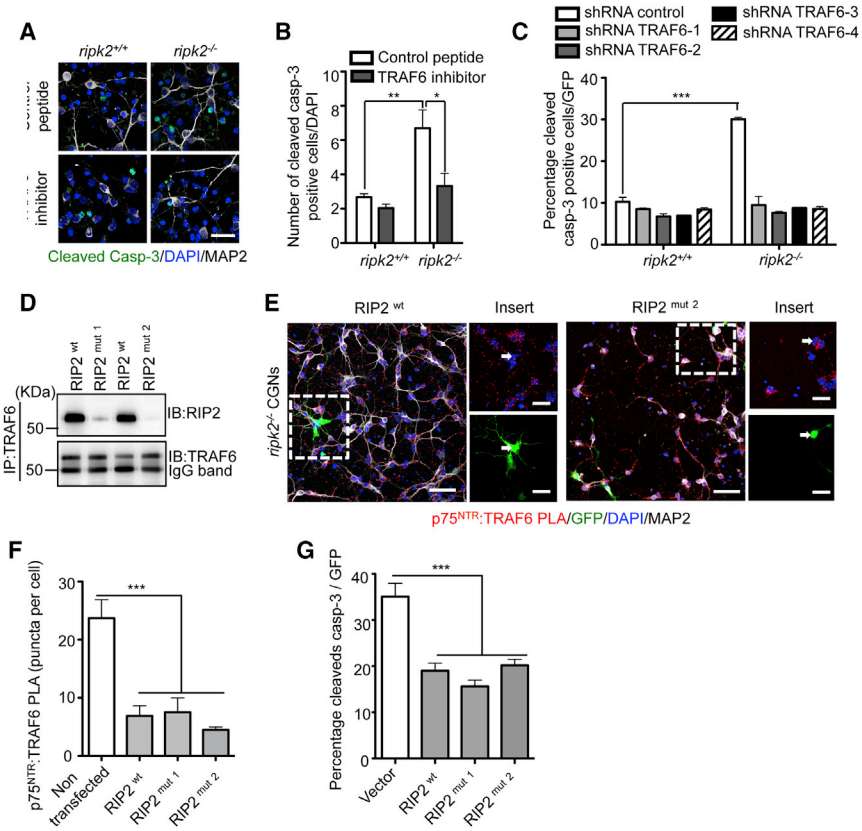

Figure 7. RIP2 and TRAF6 Compete for Binding to p75^{NTR} to Regulate CGN Survival

(A) Representative micrographs showing cleaved caspase 3 (green) in ripk2$^{+/+}$ and ripk2$^{-/-}$ CGNs cultured for 2 DIV and treated with control peptide (control Pep; 30 μM) or TRAF6 inhibitor (TRAF6in; 30 μM), counterstained for MAP2 and DAPI. Images were selected from 50 images per genotype and condition from 6 separate experiments. The scale bar represents 20 μm.

(B) Quantification of cells positive for cleaved caspase 3 in ripk2$^{+/+}$ and ripk2$^{-/-}$ CGNs treated with control peptide or TRAF6 inhibitor (decoy) peptide. Mean ± SEM of data from 4 separate cultures is shown (*p < 0.05; **p < 0.01 two-way ANOVA followed by Bonferroni test).

(C) Quantification of cells positive for cleaved caspase 3 in ripk2$^{+/+}$ and ripk2$^{-/-}$ CGNs transfected with shRNA constructs (shRNA control and TRAF6-1 to -4). Mean ± SEM of data from 3 separate cultures is shown (***p < 0.001; two-way ANOVA followed by Bonferroni test).

(D) Immunoblot analysis of TRAF6 immunoprecipitates from HEK293 cells transfected with wild-type or mutant RIP2 plasmids probed with antibodies to RIP2. Note the diminished interaction of RIP2 mutants 1 and 2 with TRAF6. The membrane was reported with antibodies to TRAF6.

(E) Micrographs of p75^{NTR}/TRAF6 PLA (red) in ripk2$^{-/-}$ CGNs transfected with RIP2 wild-type (wt) or RIP2 mutant 2 (mut2) plasmids. Images were selected from 157 images of RIP2wt and 107 images of RIP2mut2. Arrows show ripk2$^{-/-}$ CGN transfected with RIP2 plasmids. The scale bars represent 20 μm.

(F) Quantification of TRAF6 PLA puncta in ripk2$^{-/-}$ CGNs transfected with the indicated RIP2 plasmids. Mean ± SEM of data from 6 separate cultures is shown (***p < 0.001; one-way ANOVA followed by Tukey's multiple comparison test).

(G) Quantification of cells positive for cleaved caspase 3 in ripk2$^{-/-}$ CGNs treated with control peptide or TRAF6 inhibitor (decoy) peptide. Mean ± SEM of data from 3 separate cultures is shown (***p < 0.001; two-way ANOVA followed by Tukey's multiple comparison test).

and restored cell death to wild-type levels (Figures 7A and 7B). A similar result was obtained by short hairpin RNA (shRNA) knockdown of TRAF6 (Figures 7C and S5). Collectively, these results indicated that, in the absence of RIP2, enhanced binding of TRAF6 to the p75^{NTR} death receptor increases CGN cell death.

We considered two possible mechanisms by which RIP2 may gate the interaction of TRAF6 with p75^{NTR} to regulate CGN survival. As the RIP2 sequence contains a motif (PPENYE) resembling the consensus TRAF6 binding site found in several death receptors (PxxExxAr/Ac; Ar, aromatic; Ac, acidic), including p75^{NTR} (Vilar, 2017), it is possible that an interaction between RIP2 and TRAF6 hinders the latter from binding p75^{NTR}. Alternatively, RIP2 and TRAF6 may compete for binding to p75^{NTR}. Although RIP2 and TRAF6 have been shown to interact with different regions of the p75^{NTR} intracellular domain, steric hindrance may prevent their binding simultaneously to the same receptor molecule, given their relatively large size compared to the p75^{NTR} juxtamembrane and death domains. In order to address these possibilities, we generated single and double mutants of RIP2 targeting the main residues in the putative TRAF6 binding site (see Experimental Procedures). We could confirm that RIP2 and TRAF6 can interact with each other by co-immunoprecipitation after overexpression in HEK293 cells (Figure 7D). Their interaction was significantly weakened after mutation of the conserved residues in the putative TRAF6 bidding motif (Figure 7D). However, both these RIP2 mutants were indistinguishable from wild-type RIP2 at restoring the interaction of TRAF6 with p75^{NTR} (Figures 7E and 7F) and the level of cell death (Figure 7G) when overexpressed in CGNs derived from ripk2$^{-/-}$ mutant mice. These data supported the idea that RIP2 gates the interaction of TRAF6 with p75^{NTR} through a competition mechanism based on steric hindrance on the receptor itself.

DISCUSSION

Despite much research on the function of individual components in the signaling pathways regulated by death receptors, our knowledge of how these pathways are integrated and interact with each other remains scant. In this study, we describe an unexpected mechanism contributing to integrate the function of two key effectors of the p75^{NTR} death receptor, RIP2 and TRAF6, which mediate opposed functional outcomes, namely cell survival and cell death, respectively. As RIP2 and TRAF6 interact with different regions of the p75^{NTR} intracellular domain, it has been assumed that they would be able to engage the

receptor simultaneously. Unexpectedly, we uncovered a competitive interaction between these two effectors for binding to the $p75^{NTR}$, which underlies the physiological regulation of cell death among subpopulations of CGNs in the early stages of cerebellar postnatal development. In the absence of RIP2, more TRAF6 interacted with $p75^{NTR}$, leading to increased CGN cell death. This could be restored to normal levels by reintroducing RIP2, removing $p75^{NTR}$ or TRAF6, preventing TRAF6 from binding to $p75^{NTR}$, or blocking endogenously produced NGF ligands in the mutant neurons. Based on these observations, we propose that RIP2 gates the interaction of TRAF6 with $p75^{NTR}$ to balance pro-survival and pro-death pathways, thereby helping to achieve a physiological level of CGN cell death during normal cerebellar development. The pro-survival function of RIP2 downstream of $p75^{NTR}$ has been attributed to its ability to regulate the NF-κB pathway (Khursigara et al., 2001). In agreement with this, we found that mNGF was unable to regulate $p65^{NFkB}$ nuclear translocation in mutant neurons lacking RIP2. On the other hand, the increased cell death of CGNs lacking RIP2 could be restored to normal levels by blocking TRAF6, either pharmacologically or genetically, suggesting that the cell survival effects afforded by the RIP2 pathway downstream of $p75^{NTR}$ may not require regulation of NF-κB signaling and could simply be due to displacement of TRAF6 from the receptor.

In wild-type CGNs expressing RIP2, endogenously produced mNGF and proNGF displayed opposed pro-survival and pro-cell death roles, respectively, suggesting that cleavage of the NGF precursor protein, and hence the ratio between mNGF and proNGF, may be a key determinant of CGN survival in postnatal cerebellar development. Interestingly, as the proNG/mNGF ratio increased in postnatal cerebellum (Figure 1E), so did the level of RIP2 (Figure 1F), suggesting a possible mechanism to limit the surge of CGN cell death to the first two weeks of postnatal development. In the absence of RIP2, both mNGF and proNGF could induce apoptosis, explaining the enhanced cell death observed in CGNs of $ripk2^{-/-}$ mutant mice.

CGNs outnumber all other brain neurons combined and are thought to encompass heterogeneous subpopulations (Curtice et al., 2016). Recent findings have revealed their capacity of encoding complex aspects of reward and predictive information, in addition to classical sensorimotor encoding (Giovannucci et al., 2017; Wagner et al., 2017), beginning to provide an explanation for their large numbers. It would therefore seem important to understand the mechanisms that regulate CGN survival. Although deletion of neurotrophin receptors TrkB and TrkC was initially reported to enhance CGN apoptosis, these mice also showed enlargement of the granule layer and a marked increase in CGN number (Minichiello et al., 1999), suggesting alternative effects on proliferation or differentiation. Our present results show that RIP2 gates $p75^{NTR}$ signaling to affect the survival of approximately 20% of CGNs in the adult brain (estimation based on data from Figure 2I). Interestingly, CGN loss was not homogeneous across different cerebellar folia of mice lacking RIP2; e.g., although no significant difference could be found in folia VIII, over 50% cell loss was detected in folia X of the mutant mice. These results indicate a significant degree of heterogeneity in the survival requirements of CGNs and support the emerging notion of functional diversity among CGN subpopulations.

In summary, we describe a mechanism orchestrating the hierarchical activation of pro-survival and pro-cell death pathways in the $p75^{NTR}$ death receptor, which contributes to determine the number of cerebellar CGNs that survive postnatal cell death. The interplay between RIP2 and TRAF6 in $p75^{NTR}$ signaling identified in this study suggests that competitive interactions are a key feature of death receptor function.

EXPERIMENTAL PROCEDURES

Animals

Mice were housed in a 12-hr light/dark cycle and fed a standard chow diet. The following transgenic mouse lines were used: $p75^{NTR}$ knockout mice (Lee et al., 1994) and RIP2 knockout mice (Kobayashi et al., 2002). RIP2 and $p75^{NTR}$ mutant mice were maintained in a C57Bl6 background. Mice of both sexes were used for the experiments. For BrdU experiments, mice were injected with 50 mg/kg and sacrificed 2 hr, 3 days, or 7 days post-injection. Animal protocols were approved by Stockholms Norra Djurförsöksetiska Nämnd and are in accordance with the ethical guidelines of the Karolinska Institute.

Plasmids

Control shRNA and 4 unique 29-mer shRNA constructs targeting mouse TRAF6 in retroviral GFP vector plasmids were purchased from Origene. Human RIP2 in pC1 vector was obtained from Dr. Moses Chao's laboratory. Mutations in RIP2 were introduced using QuickChange Site-Directed Mutagenesis Kit (Stratagene, UK) and verified by DNA sequencing. In the TRAF6-binding site, the RIP2 wild-type sequence corresponds to IYMPPENYE, mutant 1 to IYMTPENYE, and mutant 2 to IYMTPANYE. Normal expression of all constructs and interaction to TRAF6 was verified in HEK293 cells by immunoblotting.

Cell Culture

P7 mouse cerebella were separated from the rest of the brain and placed into a plate with cold PBS. Whole cerebella or selected folia were digested with trypsin for extraction of CGNs. Folia III and X dissected under a dissection microscope following anatomical images given by Kim and Scott (2014) and White and Sillitoe (2013). CGNs were plated at a density of 40,000 cells per coverslip coated with poly-D-lysine (Sigma) in a 24-well plate (Starlab) in Basal Medium Eagle (BME) supplemented with 10% fetal calf serum (Gibco), 25 mM KCl (Sigma), 1 mM glutamine (Gibco), and 2 mg/mL gentamicin (Invitrogen). The cells were treated after 2 DIV. For assessing cleaved caspase 3, neurons were treated for 24 hr with the indicated substances and then labeled with antibodies against cleaved caspase 3 (Cell Signaling Technology; 9761; 1:400) and β-III tubulin (R&D Systems; MAB1195; 1:1,000) and counterstained with DAPI. Images were taken using a Zeiss fluorescence microscope and quantified to obtain percentage cells positive for cleaved caspase 3 relative to DAPI. To collect protein for immunoblotting, neurons were cultured at a higher density (~200,000 neurons per well) in a 48-well plate for 2 days and then serum and KCl deprived for 30 min. The neurons were then treated with the indicated substances for 15 min. To collect protein for immunoprecipitation, CGNs were cultured at higher density (~900,000 neurons per well) in 6-well plates for 2 days. Neurons were then deprived of serum and KCl for 30 min and treated with NGF for 5 min. Primary neurons from $ripk2^{+/+}$ and $ripk2^{-/-}$ mice were derived from P7 littermate pups generated by crossing heterozygous mice. CGNs were transfected after 2 DIV with Lipofectamine LTX (Invitrogen; Cat). Mouse IgG1 isotype control (MAB002) and anti-mature NGF (mNGF and MAB256) were obtained from R&D Systems. Mature NGF (N-100), brain-derived neurotrophic factor (BDNF) (B-250), and anti-NGF/proNGF (total NGF) neutralizing antibody (ALM-006) were obtained from Alomone. TRAF6 inhibitor (NBP2-26506) was obtained from Novus Biologicals. JNK inhibitor (JNK-IN-8; 420150) was purchased from Millipore. HEK293 cells were cultured in minimum essential medium Eagle (MEM) (Gibco) plus 10% fetal bovine serum (Life Technologies) supplemented with penicillin-streptomycin (Life Technologies).

Immunoprecipitation, Immunoblotting, and ELISA

Protein samples were prepared for SDS-PAGE in SDS sample buffer (Life Technologies) and boiled at 95°C for 10 min before electrophoresis on 12% polyacrylamide gels. Proteins were transferred to polyvinylidene fluoride (PVDF) membranes (Amersham). Membranes were blocked with 5% non-fat milk and incubated with primary antibodies. The following primary antibodies were used at the indicated dilutions: goat anti $p75^{NTR}$ (Neuromics; GT15057; 1:500); rabbit anti-mature NGF (Santa Cruz Biotechnology; sc-548; 1:500); mouse anti-RIP2 (BD Biosciences; 612349 and Cayman; 160783; 1:200); mouse anti-b III tubulin (R&D Systems; MAB1195; 1:10,000); phospho-c-Jun (Thr91; Cell Signal; 2303; 1:1,000); phospho-c-Jun (Ser63) II (Cell Signal; 9261; 1:1,000); rabbit anti-c-Jun (Cell Signal; 9165; 1:1,000); and mouse anti-TRAF6 (Santa Cruz; sc-8409; 1:500). Immunoreactivity was visualized using appropriate horseradish peroxidase (HRP)-conjugated secondary antibodies. Immunoblots were developed using the ECL Advance Western Blotting Detection kit (Life Technologies) and exposed to Kodak X-Omat AR films. Image analysis and quantification of band intensities were done with ImageQuant software (GE Healthcare). For immunoprecipitation, cells were lysed with RIPA buffer containing protease inhibitor (Roche) for 1 hr. Total protein was collected and incubated with anti-$p75^{NTR}$ (Neuromics; GT15057; 1:500) overnight at 4°C and then incubated with Sepharose Protein-G beads (GE Healthcare). Samples were then prepared for immunoblotting as described above. Determination of levels of secreted mature and total NGF was done using ELISA kits from Novus (for mature NGF; KA0400) or CUSABIO (for proNGF; equation 027721MO).

Immunohistochemistry, Immunocytochemistry, and *In Situ* Hybridization

For immunohistochemistry, animals were perfused with PBS followed by 4% paraformaldehyde. Brains were collected and post-fixed in 4% paraformaldehyde for 16 hr and then cryoprotected in 30% sucrose before being embedded in OCT and frozen at −80°C overnight. The tissue was serially sectioned on a cryostat at 10 or 20 μm in the sagittal plane. Midline sections were mounted onto electrostatic charged slides (Leica Microsystems), blocked with 5% donkey serum containing 0.3% Triton X-100 in PBS for 1 hr at room temperature, and then incubated for 16 hr at 4°C with primary antibodies. The sections were washed in PBS before being incubated with appropriate secondary antibody. For quantification of cleaved-caspase-3-positive cells, 10-μm sections through the cerebellum of P60 $ripk2^{+/+}$ and $ripk2^{-/-}$ animals were stained for NeuN (Millipore; MAB377; 1:200) and DAPI at the same time to ensure that they were stained in an identical manner. An area of 25,464 μm^2 for each image from folia III, VIII, and X was imaged, and the total number of NeuN-positive cells was quantified using NIH ImageJ software. For immunocytochemistry, neuron cultures were fixed in 4% paraformaldehyde and 4% sucrose for 15 min and then washed with PBS before incubation in 5% BSA and 0.3% Triton X-100 (Sigma) in PBS for 1 hr at room temperature for blocking nonspecific binding and permeabilizing the cells. Neurons were then incubated overnight with primary antibody in 1% blocking solution at 4°C. After washing with PBS, the cultures were incubated with the appropriate secondary antibody. The primary antibodies were as follows: polyclonal anti-$p75^{NTR}$ (Neuromics; GT15057; 1:200); polyclonal anti-cleaved caspase 3 (Cell Signal; 9761; 1:400); polyclonal anti-Ki67 (Novocastra; NCL-Ki67; 1:200); polyclonal anti-BrdU (Accurate Chemicals; OB0030; 1:500); monoclonal anti-NeuN (Millipore; MAB337; 1:200); monoclonal anti-β-III tubulin (R&D Systems; MAB1195; 1:10,000); polyclonal anti-MAP2 (Abcam; ab5392; 1:2,000); and polyclonal anti-GFP (Abcam; ab13970; 1:500). Secondary antibodies were Alexa-Fluor-conjugated anti-immunoglobulin from Life Technologies and Invitrogen, used at 1:1,500 (donkey anti-rabbit immunoglobulin G [IgG] Alexa Fluor 555, A31572; donkey anti-goat IgG Alexa Fluor 488, A11055; donkey anti-mouse IgG Alexa 488, A21202; donkey anti-mouse IgG Alexa Fluor 555, A31570; donkey anti-mouse IgG Alexa Fluor 647, A31571; donkey anti-goat IgG Alexa Fluor 555, A21432; and donkey anti-chicken IgG Alexa Fluor 647, Jackson, 703-496-155). Images were obtained using a Zeiss Axioplan confocal laser microscope.

Mouse RIP2 *in situ* hybridization probes were obtained by RT-PCR from P0 cerebellum (sense primer, 5′-GCTGCTCGACAGTGAAAGA-3′; antisense primer, 5′- CTCATAGTTCTCAGGTGGCATATAG-3′; Tm = 62°C) and subcloned into PCR II-TOPO-TA cloning vector (Invitrogen). The antisense probe was linearized with Spe1 and transcribed with T7 polymerase, and the sense probe was linearized with Xho1 and transcribed with Sp6 polymerase using a BIOT-NTP labeling kit (Roche). P7 pups were perfused as above. Brain tissue was collected, postfixed, and cryoprotected as above. Sagittal serial sections of 30 μm were obtained on a cryostat. Free-floating sections were washed in PBS followed by 5× saline-sodium citrate buffer (SCC) (0.75 M NaCl and 75 mM sodium citrate). The sections were then prehybridized for 2 hr at 50°C in SCC buffer containing 50% deionized formamid and 40 μg/mL salmon DNA and then incubated with sense or antisense probes at 75°C for 10 min, followed by 58°C for 16 hr. After washing at 65°C for total of 2 hr, the sections were treated with H_2O_2 to quench endogenous autofluorescence, blocked in 0.5% tyramide signal amplification solution (TSA; TSA biotin kit; PerkinElmer) for 30 min, and stained with Streptavidin-HRP (1:100) at room temperature. After several washes, the sections were incubated in biotin-tyramide (1:100) reconstituted in amplification diluent (TSA biotin kit; PerkinElmer) for 10 min. After further washes, the sections were stained with Streptavidin-488 (Life Technologies; S32354; 1:1,500) for 90 min. Sections were then washed and prepared for immunohistochemistry as described above.

Proximity Ligation Assay

After transfection or treatment, CGNs were fixed for 15 min in 4% paraformaldehyde (PFA)/4% sucrose, permeabilized, and blocked in 10% normal donkey serum and 0.3% Triton X-100 in PBS. Cells were then incubated overnight at 4°C with anti-$p75^{NTR}$ (Promega; G323A; 1:300), anti-TRAF6 (Santa Cruz; sc-8490; 1:100), and anti-MAP2 (Abcam; ab5392; 1:4,000) antibodies in PBS supplemented with 3% BSA. The Duolink *In Situ* Proximity Ligation kit (Sigma) was used as per the manufacturer's instructions with fluorophore-conjugated secondary antibody to recognize MAP2 (Molecular Probes; 703-606-155; 1:2,000) included during the amplification step. Transfected and MAP2-positive cells were imaged with an LSM Imager Z2 confocal microscope (Zeiss) to detect PLA signals. Puncta on transfected and MAP2-positive somas were quantified using NIH ImageJ software.

Behavioral Analysis

All behavioral observations and measurements were performed blind to the genotype. Six-month-old $ripk2^{+/+}$ (n = 8) and $ripk2^{-/-}$ (n = 8) mice were used for the study. As no sex differences were observed within the same genotype for any of the tests, the results of both sexes were pooled together. In all cases, mice were acclimatized to the behavioral room for at least 20 min before testing and all apparatuses were cleaned with 70% ethanol between animals. Rotarod test was performed on model 47600 (Ugo Basile) following a protocol previously described (Yamazaki et al., 2015). Mice were first subjected to 3 training sessions each of 4 training trials during 3 consecutive days. Each training trial had a maximum duration of 60 s at a fixed speed of 20 rpm with an inter-trial time of 30 min. In the test day, mice were first subjected to a 20-rpm fixed speed trial with a maximum length of 60 s followed by three trials of accelerating speed (from 4 to 40 rpm over 5 min) with a maximum length of 360 s and 1 hr inter-trial period. In all cases, a trial ended when either the mouse fell off the rod, the maximum latency was reached, or the animal rotated, hugging the rod for more than 4 rotations. For the footprint test, the hind- and forepaws of each mouse were coated with red and black nontoxic water-based paints, respectively. Mice were then allowed to walk down an enclosed runway line on a sheet of white paper. Two trials were performed in two consecutive days, and 3–6 steps from the middle portion of each run were measured for (1) stride length (average distance of forward movement between each stride), (2) forepaw and (3) hind paw base width (average distance between left and right front or hind footprints), and (4) overlap (to measure uniformity of step alternation). For evaluation of overlap, a zero value was assigned when the center of the hind footprint fell on top of the preceding front footprint. When the footprints did not overlap, the distance between the centers of the footprints was measured. In all cases, the mean values of the two trials were used for subsequent analysis.

Statistical Analysis

Data are expressed as mean and SEs. Following normality test and homogeneity variance (F-test or Kolmogorov-Smirnov test, with Dallal-Wilkinson-Lillie for p value), group comparisons were made using a unpaired Student's t test or

one-way or two-way ANOVA as appropriate, followed by Bonferroni post hoc test for normally distributed data. Mann-Whitney test was done on non-normally distributed data. Differences were considered significant when $p < 0.05$. Data from all experiments are included; no data points were excluded.

SUPPLEMENTAL INFORMATION

Supplemental Information includes Supplemental Experimental Procedures and five figures and can be found with this article online at https://doi.org/10.1016/j.celrep.2018.06.098.

ACKNOWLEDGMENTS

We thank Annika Andersson for technical support, Koichi Kobayashi for providing RIP2 knockout mice, and Moses Chao for providing RIP2 plasmid. Support for this research was provided by grants to L.K. from the Karolinska Institute Research Foundation and to C.F.I. from the European Research Council (ERC-2013-AdG-339237), the Swedish Research Council (2016-01538), the Swedish Cancer Society (CAN 2015/304), the Knut and Alice Wallenbergs Foundation (KAW 2012.0270), and the National University of Singapore (R-185-000-227-133).

AUTHOR CONTRIBUTIONS

L.K. conducted and analyzed the majority of the experiments. D.F.-S. conducted and analyzed the behavior studies. M.C.S. did preliminary gait test experiments. L.K. and C.F.I. designed the experiments and wrote the manuscript.

DECLARATION OF INTERESTS

The authors declare no competing interests.

Received: March 7, 2018
Revised: June 1, 2018
Accepted: June 22, 2018
Published: July 24, 2018

REFERENCES

Apps, R., and Strata, P. (2015). Neuronal circuits for fear and anxiety - the missing link. Nat. Rev. Neurosci. *16*, 642.

Becker, M.I., and Person, A.L. (2017). Cerebellar granule cells expand their talents. Nat. Neurosci. *20*, 633–634.

Carletti, B., and Rossi, F. (2008). Neurogenesis in the cerebellum. Neuroscientist *14*, 91–100.

Carter, B.D., Kaltschmidt, C., Kaltschmidt, B., Offenhäuser, N., Böhm-Matthaei, R., Baeuerle, P.A., and Barde, Y.-A. (1996). Selective activation of NF-kappa B by nerve growth factor through the neurotrophin receptor p75. Science *272*, 542–545.

Curtice, K.J., Leavitt, L.S., Chase, K., Raghuraman, S., Horvath, M.P., Olivera, B.M., and Teichert, R.W. (2016). Classifying neuronal subclasses of the cerebellum through constellation pharmacology. J. Neurophysiol. *115*, 1031–1042.

De Zeeuw, C.I., and Ten Brinke, M.M. (2015). Motor learning and the cerebellum. Cold Spring Harb. Perspect. Biol. *7*, a021683.

Dechant, G., and Barde, Y.-A. (2002). The neurotrophin receptor p75(NTR): novel functions and implications for diseases of the nervous system. Nat. Neurosci. *5*, 1131–1136.

Ding, Y., Li, J., Enterina, J.R., Shen, Y., Zhang, I., Tewson, P.H., Mo, G.C.H., Zhang, J., Quinn, A.M., Hughes, T.E., et al. (2015). Ratiometric biosensors based on dimerization-dependent fluorescent protein exchange. Nat. Methods *12*, 195–198.

Dollé, L., El Yazidi-Belkoura, I., Adriaenssens, E., Nurcombe, V., and Hondermarck, H. (2003). Nerve growth factor overexpression and autocrine loop in breast cancer cells. Oncogene *22*, 5592–5601.

Ferrao, R., and Wu, H. (2012). Helical assembly in the death domain (DD) superfamily. Curr. Opin. Struct. Biol. *22*, 241–247.

Foti, F., Mandolesi, L., Cutuli, D., Laricchiuta, D., De Bartolo, P., Gelfo, F., and Petrosini, L. (2010). Cerebellar damage loosens the strategic use of the spatial structure of the search space. Cerebellum *9*, 29–41.

Friedman, W.J. (2000). Neurotrophins induce death of hippocampal neurons via the p75 receptor. J. Neurosci. *20*, 6340–6346.

Friedman, W.J., Olson, L., and Persson, H. (1991). Temporal and spatial expression of NGF receptor mRNA during postnatal rat brain development analyzed by in situ hybridization. Brain Res. Dev. Brain Res. *63*, 43–51.

Geetha, T., Kenchappa, R.S., Wooten, M.W., and Carter, B.D. (2005). TRAF6-mediated ubiquitination regulates nuclear translocation of NRIF, the p75 receptor interactor. EMBO J. *24*, 3859–3868.

Giovannucci, A., Badura, A., Deverett, B., Najafi, F., Pereira, T.D., Gao, Z., Ozden, I., Kloth, A.D., Pnevmatikakis, E., Paninski, L., et al. (2017). Cerebellar granule cells acquire a widespread predictive feedback signal during motor learning. Nat. Neurosci. *20*, 727–734.

Khursigara, G., Orlinick, J.R., and Chao, M.V. (1999). Association of the p75 neurotrophin receptor with TRAF6. J. Biol. Chem. *274*, 2597–2600.

Khursigara, G., Bertin, J., Yano, H., Moffett, H., DiStefano, P.S., and Chao, M.V. (2001). A prosurvival function for the p75 receptor death domain mediated via the caspase recruitment domain receptor-interacting protein 2. J. Neurosci. *21*, 5854–5863.

Kim, B.J., and Scott, D.A. (2014). Mouse model reveals the role of RERE in cerebellar foliation and the migration and maturation of Purkinje cells. PLoS ONE *9*, e87518.

Kobayashi, K., Inohara, N., Hernandez, L.D., Galán, J.E., Núñez, G., Janeway, C.A., Medzhitov, R., and Flavell, R.A. (2002). RICK/Rip2/CARDIAK mediates signalling for receptors of the innate and adaptive immune systems. Nature *416*, 194–199.

Lee, K.-F., Davies, A.M., and Jaenisch, R. (1994). p75-deficient embryonic dorsal root sensory and neonatal sympathetic neurons display a decreased sensitivity to NGF. Development *120*, 1027–1033.

Lee, R., Kermani, P., Teng, K.K., and Hempstead, B.L. (2001). Regulation of cell survival by secreted proneurotrophins. Science *294*, 1945–1948.

Lin, Z., Tann, J.Y., Goh, E.T.H., Kelly, C., Lim, K.B., Gao, J.F., and Ibáñez, C.F. (2015). Structural basis of death domain signaling in the p75 neurotrophin receptor. eLife *4*, e11692.

Malerba, F., Paoletti, F., Bruni Ercole, B., Materazzi, S., Nassini, R., Coppi, E., Patacchini, R., Capsoni, S., Lamba, D., and Cattaneo, A. (2015). Functional characterization of human ProNGF and NGF mutants: identification of NGF P61SR100E as a "painless" lead investigational candidate for therapeutic applications. PLoS ONE *10*, e0136425.

McCarthy, J.V., Ni, J., and Dixit, V.M. (1998). RIP2 is a novel NF-kappaB-activating and cell death-inducing kinase. J. Biol. Chem. *273*, 16968–16975.

Minichiello, L., Korte, M., Wolfer, D., Kühn, R., Unsicker, K., Cestari, V., Rossi-Arnaud, C., Lipp, H.P., Bonhoeffer, T., and Klein, R. (1999). Essential role for TrkB receptors in hippocampus-mediated learning. Neuron *24*, 401–414.

Park, H.H., Logette, E., Raunser, S., Cuenin, S., Walz, T., Tschopp, J., and Wu, H. (2007). Death domain assembly mechanism revealed by crystal structure of the oligomeric PIDDosome core complex. Cell *128*, 533–546.

Pundavela, J., Roselli, S., Faulkner, S., Attia, J., Scott, R.J., Thorne, R.F., Forbes, J.F., Bradshaw, R.A., Walker, M.M., Jobling, P., and Hondermarck, H. (2015). Nerve fibers infiltrate the tumor microenvironment and are associated with nerve growth factor production and lymph node invasion in breast cancer. Mol. Oncol. *9*, 1626–1635.

Reddy, C.E., Albanito, L., De Marco, P., Aiello, D., Maggiolini, M., Napoli, A., and Musti, A.M. (2013). Multisite phosphorylation of c-Jun at threonine 91/93/95 triggers the onset of c-Jun pro-apoptotic activity in cerebellar granule neurons. Cell Death Dis. *4*, e852.

Roux, P.P., and Barker, P.A. (2002). Neurotrophin signaling through the p75 neurotrophin receptor. Prog. Neurobiol. *67*, 203–233.

Sergaki, M.C., López-Ramos, J.C., Stagkourakis, S., Gruart, A., Broberger, C., Delgado-García, J.M., and Ibáñez, C.F. (2017). Compromised survival of cerebellar molecular layer interneurons lacking GDNF receptors GFRα1 or RET impairs normal cerebellar motor learning. Cell Rep. *19*, 1977–1986.

Vicario, A., Kisiswa, L., Tann, J.Y., Kelly, C.E., and Ibáñez, C.F. (2015). Neuron-type-specific signaling by the p75NTR death receptor is regulated by differential proteolytic cleavage. J. Cell Sci. *128*, 1507–1517.

Vilar, M. (2017). Structural characterization of the p75 neurotrophin receptor: a stranger in the TNFR superfamily. Vitam. Horm. *104*, 57–87.

Vilar, M., Charalampopoulos, I., Kenchappa, R.S., Simi, A., Karaca, E., Reversi, A., Choi, S., Bothwell, M., Mingarro, I., Friedman, W.J., et al. (2009). Activation of the p75 neurotrophin receptor through conformational rearrangement of disulphide-linked receptor dimers. Neuron *62*, 72–83.

Vinueza Veloz, M.F., Zhou, K., Bosman, L.W.J., Potters, J.-W., Negrello, M., Seepers, R.M., Strydis, C., Koekkoek, S.K.E., and De Zeeuw, C.I. (2015). Cerebellar control of gait and interlimb coordination. Brain Struct. Funct. *220*, 3513–3536.

Wagner, M.J., Kim, T.H., Savall, J., Schnitzer, M.J., and Luo, L. (2017). Cerebellar granule cells encode the expectation of reward. Nature *544*, 96–100.

White, J.J., and Sillitoe, R.V. (2013). Postnatal development of cerebellar zones revealed by neurofilament heavy chain protein expression. Front. Neuroanat. *7*, 9.

Wicovsky, A., Müller, N., Daryab, N., Marienfeld, R., Kneitz, C., Kavuri, S., Leverkus, M., Baumann, B., and Wajant, H. (2007). Sustained JNK activation in response to tumor necrosis factor is mediated by caspases in a cell type-specific manner. J. Biol. Chem. *282*, 2174–2183.

Wood, K.A., Dipasquale, B., and Youle, R.J. (1993). In situ labeling of granule cells for apoptosis-associated DNA fragmentation reveals different mechanisms of cell loss in developing cerebellum. Neuron *11*, 621–632.

Yamazaki, M., Le Pichon, C.E., Jackson, A.C., Cerpas, M., Sakimura, K., Scearce-Levie, K., and Nicoll, R.A. (2015). Relative contribution of TARPs γ-2 and γ-7 to cerebellar excitatory synaptic transmission and motor behavior. Proc. Natl. Acad. Sci. USA *112*, E371–E379.

Ye, H., Arron, J.R., Lamothe, B., Cirilli, M., Kobayashi, T., Shevde, N.K., Segal, D., Dzivenu, O.K., Vologodskaia, M., Yim, M., et al. (2002). Distinct molecular mechanism for initiating TRAF6 signalling. Nature *418*, 443–447.

Yeiser, E.C., Rutkoski, N.J., Naito, A., Inoue, J., and Carter, B.D. (2004). Neurotrophin signaling through the p75 receptor is deficient in traf6-/- mice. J. Neurosci. *24*, 10521–10529.

Yoon, S.O., Casaccia-Bonnefil, P., Carter, B., and Chao, M.V. (1998). Competitive signaling between TrkA and p75 nerve growth factor receptors determines cell survival. J. Neurosci. *18*, 3273–3281.

Zanin, J.P., Abercrombie, E., and Friedman, W.J. (2016). Proneurotrophin-3 promotes cell cycle withdrawal of developing cerebellar granule cell progenitors via the p75 neurotrophin receptor. eLife *5*, 23.

Zhang, T., Inesta-Vaquera, F., Niepel, M., Zhang, J., Ficarro, S.B., Machleidt, T., Xie, T., Marto, J.A., Kim, N., Sim, T., et al. (2012). Discovery of potent and selective covalent inhibitors of JNK. Chem. Biol. *19*, 140–154.

Cell Reports, Volume *24*

Supplemental Information

RIP2 Gates TRAF6 Interaction with Death Receptor $p75^{NTR}$ to Regulate Cerebellar Granule Neuron Survival

Lilian Kisiswa, Diana Fernández-Suárez, Maria Christina Sergaki, and Carlos F. Ibáñez

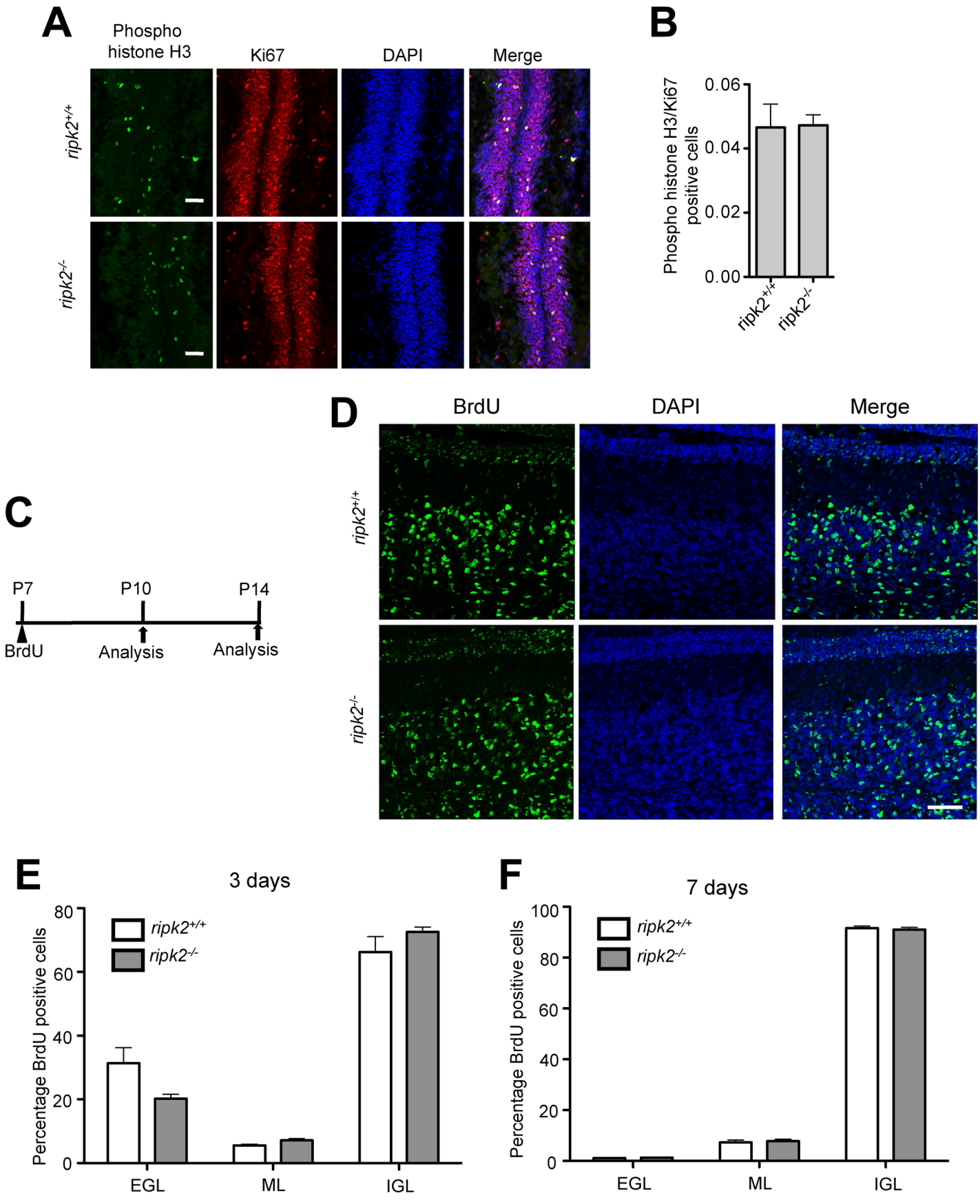

Figure S1. CGN migration is not impaired in ripk2-/- mice. Related to Figure 2.
(A) Representative images of cerebellar sections from P7 ripk2+/+ and ripk2−/− mice labeled with antibodies against phospho-histone H3 and Ki67, counterstained with DAPI. Scale bars, 50 μm.
(B) Ratio of phospho-histone H3 over Ki67 positive cells in cerebellar sections from P7 ripk2+/+ and ripk2−/− mice . Mean ± s.e.m. of data from 5 ripk2+/+ and 5 ripk2−/− mice per group.
(C) Schematic diagram of experimental setup for BrdU injection and analysis.
(D) Representative images of BrdU positive cells in cerebellum of ripk2+/+ and ripk2−/− mice 7 after days BrdU pulse and. Scale bar, 50 μm.
(E-F). Quantification of percentage of BrdU positive cells after 3 days (E) and 7 days (F) BrdU pulse. Mean ± s.e.m. of data from 5 animals per genotype.

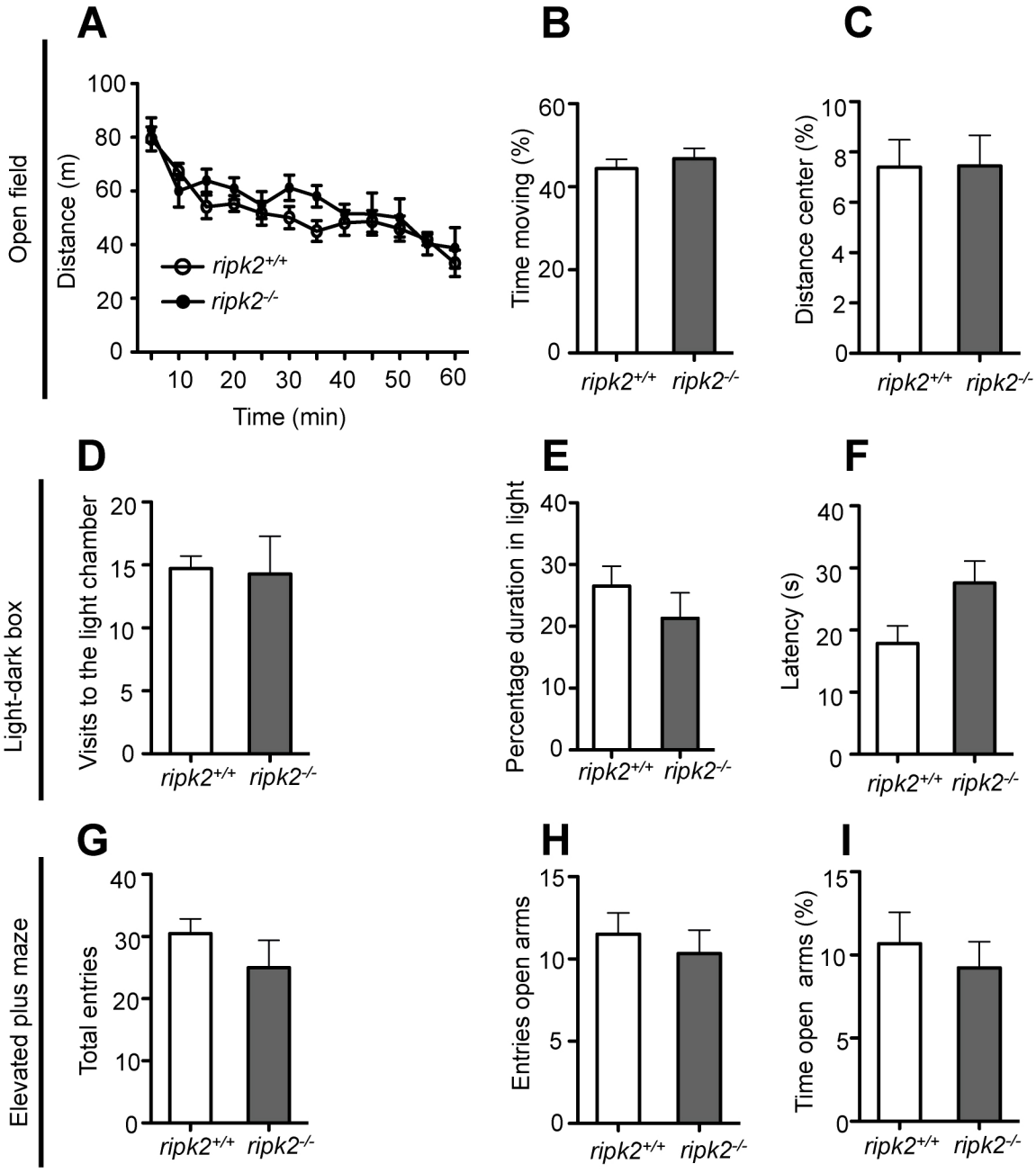

Figure S2. Open field test, light-dark box test and elevated plus maze test. Related to Figure 3.

(A-C) Open field test showing distance animals travelled (A), time spent moving (B), distance spent in center (C). Mean ± s.e.m. of data from 7 ripk2+/+ and 7 ripk2−/− mice at 6 months old.

(D-F) Light-dark box test showing visits (D), time spent (E) and latency to entry (F) to light chamber in ripk2+/+ and ripk2−/− mice. Mean ± s.e.m. of data from 7 ripk2+/+ and 7 ripk2−/− mice at 6 months old.

(G-I) Elevated plus-maze test showing total entries (G), entries to the open arms (H) and time spent in the open arms (I) in ripk2+/+ and ripk2−/− mice. Mean ± s.e.m. of data from 877 ripk2+/+ and 7 ripk2−/− mice at 6 months old.

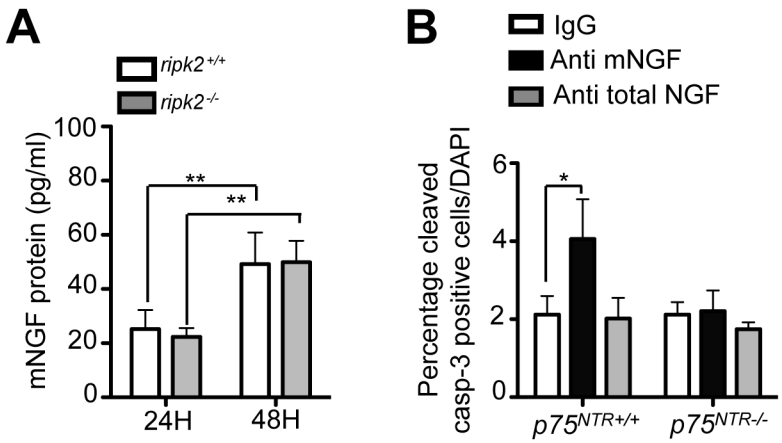

Figure S3. mNGF secretion from ripk2−/− mutant CGNs and cell death in cultures of p75NTR−/− mutant CGNs. Related to Figure 4.

(A) Concentration of secreted mNGF by cultured ripk2+/+ and ripk2−/− CGNs at a density 500,000 neurons per well in a 48-well plate. Mean ± s.e.m. of data from five separate cultures (**, P < 0.01 compared to control, unpaired Student t-test).

(B) Percentage cells positive for cleaved caspase 3 in cultured CGNs from p75NTR+/+ and p75NTR−/− mice treated with IgG control (1 μg/ml), anti mNGF (1 μg/ml) or anti total NGF (1 μg/ml) antibodies for 24 hs. Mean ± s.e.m. of data from five separate cultures per genotype and condition (*, P < 0.05; two-way ANOVA followed by Benferroni test).

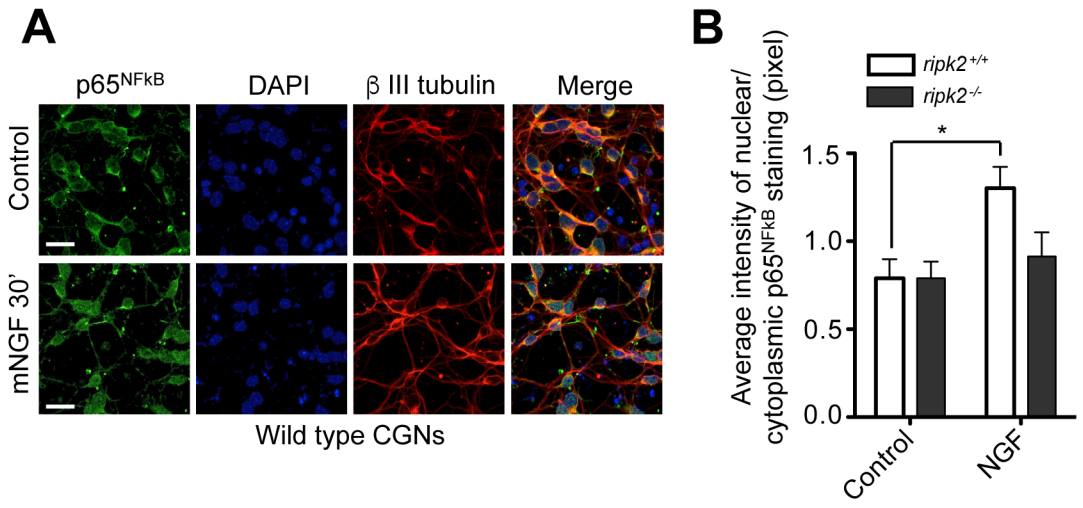

Figure S4. Deficient nuclear translocation of p65NFkB subunit in response to NGF in ripk2−/− mutant CGNs. Related to Figure 6.

(A) Representative images cultured P7 CGNs treated with vehicle (control) or NGF (100ng/ml) for 30 min and labeled with anti-p65NFkB (green) and β III tubulin (red) antibodies and counterstained with DAPI (blue). Scale bars, 20μm.

(B) Quantification of p65NFkB nuclear translocation in cells treated with vehicle (control) or NGF. Mean ± s.e.m. of results from 4 separate cultures are shown (*, $P < 0.05$ compared to control, unpaired Student t-test).

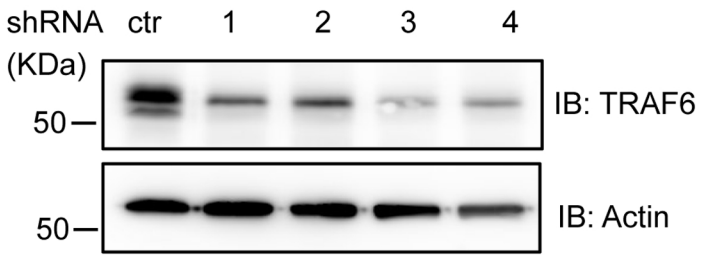

Figure S5. Knock-down of TRAF 6 expression with shRNAs. Related to Figure 7. Immunoblot of TRAF6 expression (reprobed with antibodies to actin) in lysates of HEK293 cells transfected with mouse TRAF6 expression plasmid along with different shRNAs constructs. ctr, control of scrambled shRNA. 1 to 4 denote 4 different shRNA constructs against mouse TRAF6.

Supplemental Experimental Procedures

For the open field test, mice were placed in the center of a 48cm x 48cm transparent acrylic box equipped with lightbeam strips (TSE Actimot system) and allowed to move freely for 60 min. General locomotor parameters including distance travelled, time moving, distance in the center and rearing were calculated using Actimot Software. For the lght-dark box test, the TSE Actimot system compartment was divided in two areas of the same size by inserting a dark box (24cm x 48cm) connected to the other half of the chamber by a 6x6 cm passageway. A white neon lamp was placed on top of the equipment to illuminate the open side of the arena. Mice were placed in the dark chamber and their movements were recorded for 5 min. The number of transitions, the latency to go to the light and the time spent in each chamber was analyzed using the Actimot software. For the elevated-plus maze, the apparatus consisted of a cross-shaped maze with two open arms and two closed arms (25 cm long) elevated 70 cm above the floor. Each animal was placed in the central square facing one of the open arms and the movement of each mouse was recorded over 5 min using an infrared camera. The number of entries and the staying time in each of the arms were analysed using the EthoVision software (Noldus).